Dissipation in cone-jet electrosprays and departure from isothermal operation

M. Gamero-Castaño

Phys. Rev. E **99**, 061101 — Published 26 June 2019

DOI: 10.1103/PhysRevE.99.061101

Dissipation in Cone-Jet Electrosprays and Departure from Isothermal Operation

M. Gamero-Castao
Department of Mechanical and Aerospace Engineering,
University of California, Irvine, California 92697
(Dated: April 16, 2019)

Electrospraying in the cone-jet mode has being regarded an isothermal process, and the laws obtained under this assumption are considered valid throughout the operational range. However self-heating due to dissipation is expected to be significant at sufficiently high electrical conductivities. This is confirmed by solving the isothermal leaky-dielectric model to evaluate the ohmic and viscous dissipation, and estimate the temperature increase. Self-heating is important at conductivities $\gtrsim 0.05$ S/m, increases rapidly at larger values, and requires the non isothermal modeling of this regime.

Electrospraying is an atomization technique characterized by the strong interaction between electrostatic, capillary and viscous stresses on a liquid meniscus, resulting in the formation of a charged jet and droplets. Electrosprays can be operated in a variety of modes such as cone-jet, dripping, electrospinning and coaxial [1–3], and are used in applications as diverse as electric propulsion for spacecraft [4], drug encapsulation [5], generation of fibers for tissue engineering [6], etc. Cone-jets are characterized by the conical shape of the meniscus, the long and steady jet that originates from its apex, and the generation of fine sprays. The diameters of the jet and droplets are controllable down to a few nanometers through the physical properties of the liquid and its flow rate Q. This ability has motivated substantial fundamental research, which has yielded scaling laws [7, 8] for key observables such as the total emitted current and the diameters of the jet and droplets, and detailed numerical solutions of continuum models [9–11]. These models do not consider heating due to dissipation, and assume isothermal flow. However retarding potential measurements of droplets suggest that an important fraction of the electric power injected in the electrospray is dissipated, causing significant self-heating in cone-jets of liquids with high electrical conductivities [12]. The goal of this letter is to confirm this hypothesis, and determine the conditions under which the isothermal assumption breaks down.

We quantify the dissipation by solving the isothermal equations of the leaky dielectric model particularized to cone-jets, and evaluating the ohmic P_Ω and viscous P_μ dissipation with the solution. The computed dissipation is then used to estimate the increase in the temperature of the fluid. While this approach is valid to determine the onset of self-heating, accurate modeling of the temperature field and/or of more intense self-heating conditions requires a non-isothermal treatment of the leaky dielectric model and the inclusion of the equation of energy. Fig. 1 shows a picture of a cone-jet. When the diameter of the jet is much smaller than the base of the cone, observables such as the total emitted current I and droplet distributions do not depend on the geometry and potential of the electrodes, but are largely determined by the local distribution of charge in the transition from cone to jet [7]. The dimensionless solution is then a function of three parameters, typically the dimensionless flow rate $\Pi_Q = \frac{\rho K Q}{\gamma \varepsilon_o}$, the Reynolds number $Re = (\frac{\rho \varepsilon_o \gamma^2}{\mu^3 K})^{1/3}$, and the dielectric constant ε; ρ, K, γ, and μ, are the density, electrical conductivity, surface tension and viscosity of the liquid, and ϵ_o is the vacuum permittivity. Our model takes advantage of this by restricting the simulation region to a smaller zone centered in the apex (e.g. the circle inside the white circumference in Fig. 1), and imposing the analytical Taylor potential [13] as the far-field boundary condition [14]. The leaky dielectric model with constant fluid properties (isothermal assumption) includes the equations of conservation of mass and charge, Navier-Stokes, and the Laplace equations for the electrical potentials in the fluid and surrounding vacuum [9, 15, 16],

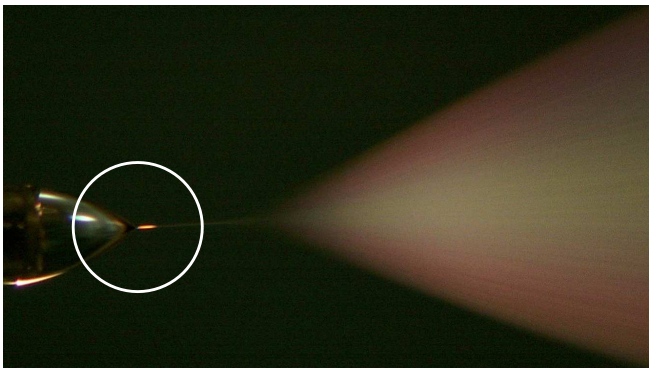

FIG. 1. Picture of a cone-jet and spray of droplets. The white circle encloses the typical simulation domain.

$$\nabla \cdot \boldsymbol{v} = 0, \quad \boldsymbol{v} \cdot \nabla \boldsymbol{v} = -\frac{\pi^2}{\Pi_Q^{1/2}} \nabla p + \frac{\pi}{\Pi_Q^{1/2} Re} \nabla^2 \boldsymbol{v} \qquad (1)$$

$$\nabla^2 \phi^i = 0, \quad \nabla^2 \phi^i = 0, \qquad (2)$$

$$\frac{d}{dx}(R v_s \sigma) = 2 R E_n^i (1 + R'^2)^{1/2}. \qquad (3)$$

The variables of the model are the velocity $\boldsymbol{v}$ and pressure p fields in the liquid, the position of the free surface $R(x)$,

the surface charge $\sigma(x)$, and the potential fields inside ϕ^i and outside ϕ^o the liquid (the electric field is given by $\boldsymbol{E} = -\nabla\phi$). v_s stands for the surface velocity, E_n and E_t for the components of $\boldsymbol{E}$ normal and tangential to the surface, and x and r for the axial and radial cylindrical coordinates. The equations are made dimensionless with the scales $r_c = (\frac{\rho\varepsilon_o Q^3}{\gamma K})^{1/6}$, $v_c = \frac{Q}{\pi r_c^2}$, $p_c = \frac{\gamma}{r_c}$, $I_c = (\gamma K Q)^{1/2}$, $E_c = \frac{I_c}{\pi r_c^2 K}$, $\phi_c = r_c E_c$, and $\sigma_c = \frac{I_c}{2\pi r_c v_c}$. Henceforth symbols capped with a tilde will designate dimensional variables. Additional constraints include the balance of stresses on the surface along the normal $\boldsymbol{n}$ and tangential $\boldsymbol{t}$ directions

$$\nabla\cdot\boldsymbol{n} = p + \frac{2}{\pi Re}\boldsymbol{n}\cdot\tau_\mu\cdot\boldsymbol{n} + \frac{1}{2\pi^2\Pi_Q^{1/2}}\{E_n^{o2} - \varepsilon E_n^{i2} + (\varepsilon-1)E_t^2\} \tag{4}$$

$$\boldsymbol{t}\cdot\tau_\mu\cdot\boldsymbol{n} = \frac{Re}{2}\sigma E_t \tag{5}$$

(τ_μ is the viscous stress tensor), the kinematic velocity condition and the jump of the normal component of the electric field at the surface

$$\boldsymbol{v}\cdot\boldsymbol{n} = 0, \quad \sigma = \frac{2}{\pi\Pi_Q^{1/2}}(E_n^o - \varepsilon E_n^i). \tag{6}$$

A velocity field is prescribed at the inlet (sink flow with a flow rate Q), and the Taylor potential is imposed as the electrostatic far-field boundary condition,

$$\phi_T(x,r) = -4.23\Pi_Q^{1/4}(x^2+r^2)^{1/4}P_{1/2}(\frac{x}{\sqrt{x^2+r^2}}). \tag{7}$$

$P_{1/2}$ is the Legendre function of the first kind of degree $\frac{1}{2}$. Finally, the ohmic and viscous dissipation densities are evaluated with the numerical solution:

$$\tilde{P}_\Omega''' = K\tilde{E}^2, \quad \tilde{P}_\mu''' = \tilde{\tau}_\mu : \nabla\tilde{\boldsymbol{v}} \tag{8}$$

Ref. [11] describes in detail the model and numerical algorithm, and validates the solution with measurements. The operational conditions studied in this letter include two dielectric constants, 8.91 and 64.9, i.e. the liquids tributyl phosphate and propilene carbonate respectively; two Reynolds numbers for each dielectric constant (0.29 and 1.12 for $\varepsilon = 8.91$, and 0.40 and 0.74 for $\varepsilon = 64.9$); and a wide range of flow rates for each Reynolds.

Figure 2(a) shows features of a typical solution for $\Pi_Q = 96.6$, $Re = 0.397$ and $\varepsilon = 64.9$: the position of the surface, the surface current $\tilde{I}_S(x) = 2\pi\tilde{R}\tilde{v}_s\tilde{\sigma}$, the bulk conduction current $\tilde{I}_B(x) = \int_0^{\tilde{R}} 2\pi\tilde{r}K\tilde{E}_x^i d\tilde{r}$, and the ohmic and viscous dissipation linear densities, $\tilde{P}'(x) = \int_0^{\tilde{R}} 2\pi\tilde{r}\tilde{P}'''d\tilde{r}$. Charge conservation requires the sum of $\tilde{I}_B(x)$ and $\tilde{I}_S(x)$ to be constant and equal to the total current I. The large cross section of the cone requires negligible velocities and an electrostatic field upstream. As the fluid approaches the apex the increasing

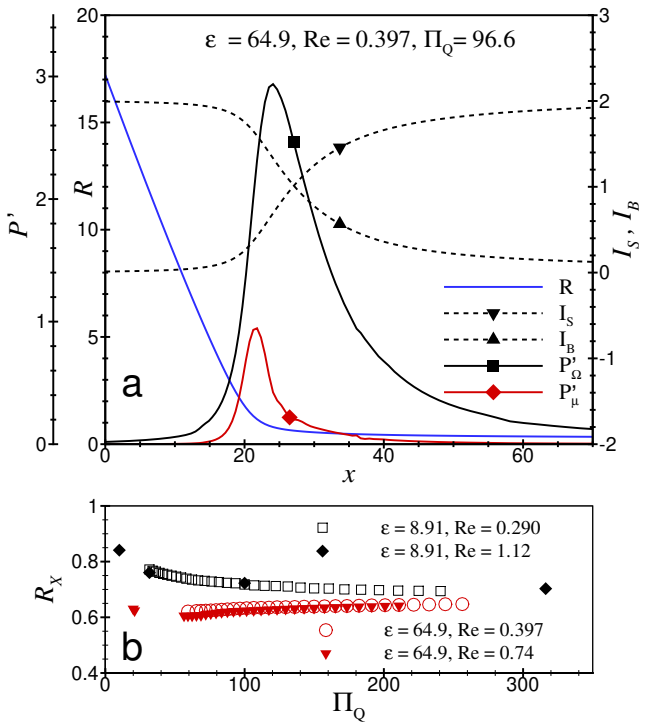

FIG. 2. (a) Features of a typical numerical solution. (b) Radius of the jet at the current crossover point.

convection tends to lower the surface charge below its equilibrium value, $\tilde{\sigma}_{eq} = \varepsilon_o\tilde{E}_n^o$, and an electric field inside the fluid must develop to inject charge on the surface and restore equilibrium. The zone where bulk current transforms into surface current is known as the transition region, and the meniscus evolves into a jet within it. The ohmic dissipation is larger than viscous dissipation. They peak nearby, $\tilde{P}'_\mu$ closer to the point x_o where $R''(x)$ is maximum, $x_o = 20.7$, while $\tilde{P}'_\Omega$ peaks further downstream just before the current crossover, $x_X = 27.1$. $\tilde{P}'_\mu$ falls off faster than $\tilde{P}'_\Omega$ downstream from the peak. An important feature is the weak dependence of the geometry of the transition region on the three dimensionless numbers parametrizing the solution [11]. For example Fig. 2(b) shows the dimensionless radius at the current crossover, R_X, which depends only slightly on Re, Π_Q and ε in a wide range of the parameters.

Figure 3 shows the total ohmic dissipation in the transition region as a function of Π_Q, calculated as:

$$P_\Omega = \frac{1}{I_c\phi_c}\int_{-\infty}^{x_f}\tilde{P}'_\Omega d\tilde{x}. \tag{9}$$

where the exit point of the transition region x_f is such that the surface current reaches 95% of the total current. For the present analysis P_Ω can be regarded a function of Π_Q only, and the power law

$$P_\Omega \cong 7.30\Pi_Q^{0.41} \tag{10}$$

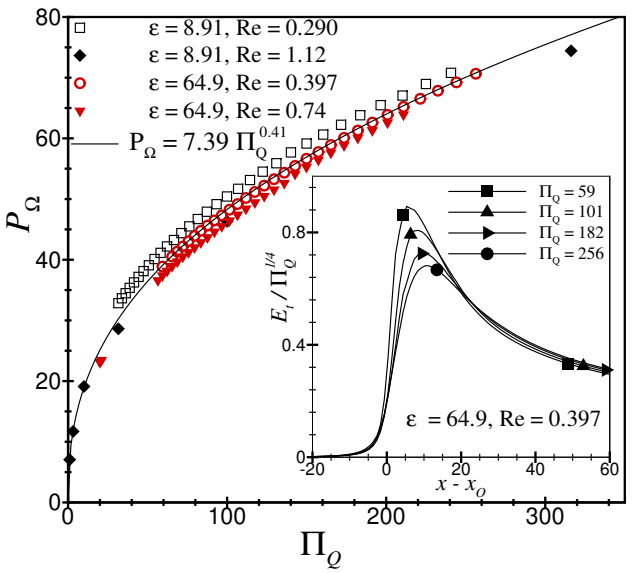

FIG. 3. Total ohmic dissipation in the transition region and tangential electric field profiles exhibiting the $\Pi_Q^{1/4}$ scaling.

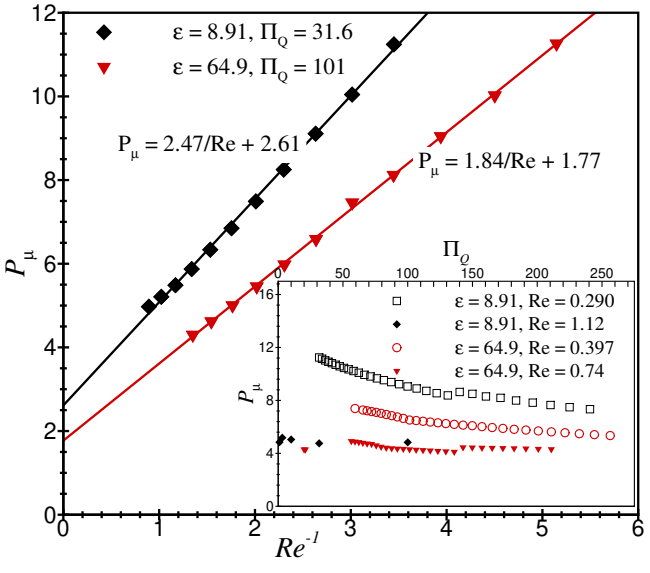

FIG. 4. Total viscous dissipation and dependency on the dimensionless numbers parameterizing the solution.

approximates well all values. To explain this we notice that the integral of the dissipation density is done over a volume that depends weakly on Π_Q, Re and ε. Thus the total dissipation scales with the square of the electric field inside the liquid, which in the transition region is well approximated by E_t^2 due to the smallness of the ratio $(E_n^i/E_t)^2$ and the quasi one-dimensional geometry. Therefore, the power law (10) suggests a scaling $E_t \sim \Pi_Q^{0.2}$. This observation seems contradictory because E_t exhibits a maximum near the current crossover that scales as $E_{t,max} \cong I/(2R_X^2)$, and both I and R_X are weak functions of Π_Q. In fact, power fits yield $E_{t,max} \cong 1.93\Pi_Q^{0.06}$ for $\varepsilon = 64.9$, and $E_{t,max} \cong 1.76\Pi_Q^{0.09}$ for $\varepsilon = 8.91$ [11]. On the other hand Taylor's potential, Eq. (7), scales as $\Pi_Q^{1/4}$ and if this scaling remained valid through most of the transition region it would explain Eq. (10). This is tested in the inset of Fig. 3, which shows $E_t(x)/\Pi_Q^{1/4}$ for several flow rates, $\varepsilon = 64.9$ and $Re = 0.397$. $E_{t,max}$ is a weak function of Π_Q ($E_{t,max} \cong 1.93\Pi_Q^{0.06}$), but on both sides of the maximum the field rapidly converges to a law that scales as $\Pi_Q^{1/4}$. Since the interval where this scaling holds corresponds to the largest fraction of the area under $P'_\Omega(x)$ (see Fig. 2(a)), while the $\Pi_Q^{0.06}$ scaling only influences a narrower section near the peak, P_Ω must scale with a power of Π_Q slightly smaller than 1/2, as found in Fig. 3. The very rapid convergence of the electric field to the $\Pi_Q^{1/4}$-dependence of Taylor's potential is surprising, and is not the artifact of imposing the far field boundary condition unreasonably close to the apex: in these calculations it is imposed on a circumference with a radius of 200.5 units centered at $x = 0$, and selected simulations using a radius of 2005 units yield no significantly different solutions.

Figure 4 plots the total viscous dissipation. P_μ is proportional to Re^{-1}, and a weaker function of Π_Q and ε. These dependencies can be explained by writing the volume integral in dimensionless form:

$$P_\mu = \frac{1}{\pi Re}\int_{-\infty}^{x_f}\int_0^{R(x)} (\tau_\mu : \nabla \boldsymbol{v}) 2\pi r dr dx. \qquad (11)$$

The Re^{-1} dependency is a consequence of the proportionality between viscous stress and viscosity. On the other hand and due to the quasi one-dimensionality of the transition region, $2v_{x,x}^2$ is the dominant term in $\tau_\mu : \nabla \boldsymbol{v}$ while the axial component of the velocity is well approximated by $v_x \cong R^{-2}$. Thus the dependence of the integral on Π_Q and ε is directly associated with the dependence of the geometry of the transition region on these two parameters, which is small. From this discussion and as shown in Fig. 2(a), most of the viscous dissipation occurs where $R'(x)$ changes most abruptly, i.e. at the base of the jet. The sharpness of this transition is governed by the ratio between the electrical relaxation time and the fluid residence time, given by $\varepsilon/\Pi_Q^{1/2}$ [11]. When $\varepsilon/\Pi_Q^{1/2} \gg 1$ the surface charge is far from equilibrium and the conical shape of the meniscus continues farther into the axis, making the transition sharper and increasing the dissipation. Conversely when $\varepsilon/\Pi_Q^{1/2} \ll 1$ the surface charge is in equilibrium and the free surface must separate upward from the conical shape earlier, making the transition smoother and decreasing the dissipation. The moderate decrease of P_μ at increasing Π_Q in the inset of Fig. 4 is consistent with this. For simplicity we

will disregard this weaker dependence and use

$$P_\mu \cong \alpha Re^{-1} + \beta \tag{12}$$

where α and β are of order one and depend on the dielectric constant of the liquid.

To determine when self-heating becomes important we notice that the Peclet number is large, $Pe = \rho c_p r_c v_c/k = \pi^{-1}(\mu c_p/k) Re \Pi_Q^{1/2}$, making thermal diffusion negligible. Thus, as the fluid moves downstream the temperature increase can be approximated as $\rho c_p Q \Delta\tilde{T}(x) \cong \tilde{P}(x)$:

$$\Delta\tilde{T} \cong \frac{\gamma^2}{\pi c_p \mu^2}\frac{1}{Re^2}\left(\frac{7.30}{\Pi_Q^{0.09}} + \frac{\alpha}{\Pi_Q^{1/2} Re} + \frac{\beta}{\Pi_Q^{1/2}}\right) \tag{13a}$$

$$= \frac{\gamma}{\pi\rho c_p}\frac{1}{r_c}\left(7.30\Pi_Q^{0.41} + \frac{\alpha}{Re} + \beta\right). \tag{13b}$$

(13a) casts the temperature increase in terms of the physical properties of the liquid, in particular the ratio $\frac{\gamma^2}{c_p\mu^2}$ and the Reynolds number; viscous dissipation is still a small fraction of the total when self-heating starts to be significant, while the exponent 0.09 reduces the effect of a varying Π_Q. The most obvious consequence of self-heating is the increase of the electrospray current at constant flow rate due to the increase of the electrical conductivity with temperature: the current follows the well-established scaling law [7, 8]

$$\tilde{I}/I_o \propto \Pi_Q^{1/2}, \tag{14}$$

with $I_o = \sqrt{\varepsilon_0\gamma^2/\rho}$, while the electrical conductivity is the factor in Π_Q most sensitive to temperature. Using Walden's rule $K\mu = constant$ [17] to relate conductivity and viscosity, whose temperature dependence is more commonly tabulated, and the scaling law for the current, small changes in temperature and current are related by:

$$\Delta\tilde{T} \cong -\frac{2\mu}{d\mu/d\tilde{T}}\frac{\Delta\tilde{I}}{\tilde{I}}. \tag{15}$$

Using a 5% current increase as the criterion for the onset of significant self-heating, values of the physical properties at 25 ^oC [18], and Eq. (15), the resulting temperature increases for tributyl phosphate, propylene carbonate, ethylene glycol and formamide (liquids typically used in electrospraying) are 5.5 ^oC, 5.5 ^oC, 2.5 ^oC and 3.6 ^oC respectively. The associated Reynolds numbers and electrical conductivities obtained with Eq. (13a) are 0.15, 0.26, 0.068 and 0.28, and 0.051 S/m, 0.064 S/m, 0.014 S/m and 0.041S/m respectively; although we use a typical value of 40 for Π_Q, note that (13a) is nearly independent of Π_Q. Eq. (13b) emphasizes the relationship between temperature increase and the characteristic radius of the jet and droplets. For the same liquids and using again $\Pi_Q = 40$, the values of r_c at the onset of self-heating are 60 nm, 55 nm, 161 nm and 85 nm respectively.

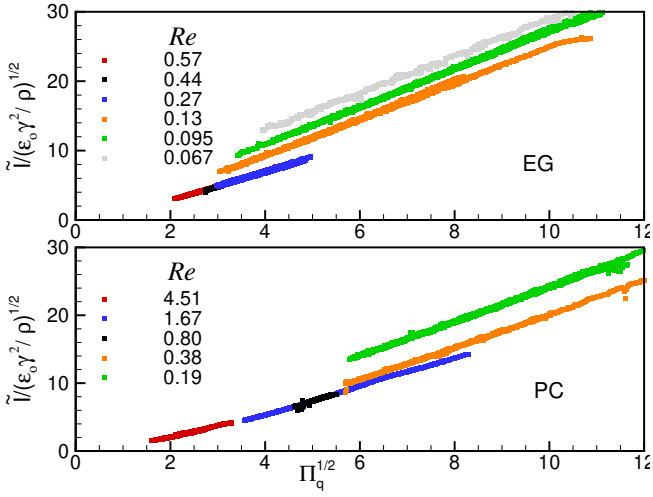

FIG. 5. Current vs flow rate measurements of ethylene glycol (EG) and propilene carbonate (PC) solutions at varying Re. The breakdown of the $\tilde{I}/I_o \propto \Pi_Q^{1/2}$ law at sufficiently low Reynolds number is indicative of self-heating.

Fig. 5 provides indirect experimental confirmation of the onset of significant self-heating by plotting measurements of the current and flow rate for solutions of propylene carbonate and ethylene glycol at decreasing Reynolds, or equivalently at increasing electrical conductivity. For a given liquid, i.e. at fixed dielectric constant, all evidence to date indicates that the dimensionless current $\tilde{I}/I_o$ only depends on the dimensionless flow rate, it follows the scaling law (14), and does not depend on the Reynolds number [7, 8, 11]. While the propylene carbonate solutions with $Re \geq 0.80$ exhibit these features, the data for $Re = 0.38$ is above the scaling law (14), and the separation increases considerably for $Re = 0.19$. Furthermore the one-to-one correspondence between dimensionless current and flow rate breaks down. The same departure from the expected behavior occurs for ethylene glycol when $Re \leq 0.13$. The failure of the scaling law (14) is consistent with the onset of self-heating: first, it occurs near the values of Re predicted by Eq. (13a). Second, although the temperature increases monotonically downstream, an effective temperature can be defined to estimate the physical properties in the definitions of Π_Q and I_o. The viscosity and the electrical conductivity are by far the properties most sensitive to temperature, with K increasing with T. Thus the effect of the temperature increase is to make Π_Q larger ($\Pi_Q \propto K$), while $\tilde{I}/I_o$ remains unchanged. Therefore, when correcting for the increased temperature, the $\{\Pi_Q^{1/2}, \tilde{I}/I_o\}$ points above the expected trend will shift towards increasing $\Pi_Q^{1/2}$ at constant $\tilde{I}/I_o$, i.e. in the direction of the isothermal scaling law.

In conclusion, self-heating due to ohmic and viscous dissipation is a key feature of electrosprays in the cone-

jet mode at sufficiently low Reynolds numbers. The electrical conductivity at which significant self-heating starts taking place depends on the liquid, especially on its viscosity, and a value of 0.05 S/m can be used as an approximate value. Cone-jets of liquids with higher conductivities will exhibit non-homogeneous temperatures and physical properties (especially the viscosity and the electrical conductivity), which invalidate the use of existing isothermal models and scaling laws in this regime. Besides its effect on the electrohydrodynamics of cone-jets, self-heating has a major influence in the field evaporation of ions from the surface of cone-jets typical of highly conducting liquids $K \gtrsim 0.1$ S/m [19], and will need to be accounted for in the evaluation of this phenomenon.

This research was supported by NASAs Space Technology Research Early Stage Innovations program, grant NNX17AD01G.

[1] M. Cloupeau and B. Prunet-Foch, Journal of Electrostatics **25**, 165 (1990).
[2] D. H. Reneker and I. Chun, Nanotechnology **7**, 216 (1996).
[3] I. G. Loscertales, A. Barrero, I. Guerrero, R. Cortijo, M. Marquez, and A. M. Gañán-Calvo, Science **295**, 1695 (2002).
[4] M. Gamero-Castaño and V. Hruby, Journal of Propulsion and Power **17**, 977 (2001).
[5] F. Mei and D.-R. Chen, Physics of Fluids **19**, 103303 (2007).
[6] T. A. Sill and H. A. von Recum, Biomaterials **29**, 1989 (2008).
[7] J. Fernandez de la Mora and I. Loscertales, Journal of Fluid Mechanics **260**, 155 (1994).
[8] A. Gañán-Calvo, J. López-Herrera, M. Herrada, A. Ramos, and J. Montanero, Journal of Aerosol Science **125**, 32 (2018).
[9] F. Higuera, Journal of Fluid Mechanics **484**, 303 (2003).
[10] M. A. Herrada, J. M. Lopez-Herrera, A. M. Gañan-Calvo, E. J. Vega, J. M. Montanero, and S. Popinet, Physical Review E - Statistical, Nonlinear, and Soft Matter Physics **86**, 026305 (2012).
[11] M. Gamero-Castano and M. Magnani, Journal of Fluid Mechanics **859**, 247 (2019).
[12] M. Gamero-Castaño, Journal of Fluid Mechanics **662**, 493 (2010).
[13] G. Taylor, Proceedings of the Royal Society of London A: Mathematical, Physical and Engineering Sciences **280**, 383 (1964).
[14] A. M. Gañán-Calvo, Physical Review Letters **79**, 217 (1997).
[15] J. R. Melcher and G. I. Taylor, Annual Review of Fluid Mechanics **1**, 111 (1969).
[16] D. A. Saville, Annual Review of Fluid Mechanics **29**, 27 (1997).
[17] P. Longinotti and H. Corti, Journal of Physical Chemistry B **113**, 5500 (2009).
[18] J. Riddick, W. Bunger, and T. Sakano, *Organic solvents: physical properties and methods of purification. Fourth edition*, Techniques of chemistry, Vol. II (Wiley-Interscience, 1986).
[19] M. Gamero-Castaño, Physical Review Letters **89**, 147602 (2002).